NASA/TM–2016–218974

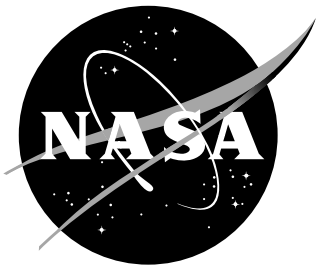

Compressive Testing of Stitched Frame and Stringer Alternate Configurations

Frank A. Leone, Jr.
NASA Langley Research Center, Hampton, VA

Dawn C. Jegley
NASA Langley Research Center, Hampton, VA

April 2016

NASA STI Program ... in Profile

Since its founding, NASA has been dedicated to the advancement of aeronautics and space science. The NASA scientific and technical information (STI) program plays a key part in helping NASA maintain this important role.

The NASA STI Program operates under the auspices of the Agency Chief Information Officer. It collects, organizes, provides for archiving, and disseminates NASA's STI. The NASA STI Program provides access to the NTRS Registered and its public interface, the NASA Technical Reports Server, thus providing one of the largest collections of aeronautical and space science STI in the world. Results are published in both non-NASA channels and by NASA in the NASA STI Report Series, which includes the following report types:

- TECHNICAL PUBLICATION. Reports of completed research or a major significant phase of research that present the results of NASA programs and include extensive data or theoretical analysis. Includes compilations of significant scientific and technical data and information deemed to be of continuing reference value. NASA counterpart of peer-reviewed formal professional papers, but having less stringent limitations on manuscript length and extent of graphic presentations.
- TECHNICAL MEMORANDUM. Scientific and technical findings that are preliminary or of specialized interest, e.g., quick release reports, working papers, and bibliographies that contain minimal annotation. Does not contain extensive analysis.
- CONTRACTOR REPORT. Scientific and technical findings by NASA-sponsored contractors and grantees.
- CONFERENCE PUBLICATION. Collected papers from scientific and technical conferences, symposia, seminars, or other meetings sponsored or co-sponsored by NASA.
- SPECIAL PUBLICATION. Scientific, technical, or historical information from NASA programs, projects, and missions, often concerned with subjects having substantial public interest.
- TECHNICAL TRANSLATION. English-language translations of foreign scientific and technical material pertinent to NASA's mission.

Specialized services also include organizing and publishing research results, distributing specialized research announcements and feeds, providing information desk and personal search support, and enabling data exchange services.

For more information about the NASA STI Program, see the following:

- Access the NASA STI program home page at ***http://www.sti.nasa.gov***
- E-mail your question to help@sti.nasa.gov
- Phone the NASA STI Help Desk at 757-864-9658
- Write to:
  NASA STI Information Desk
  Mail Stop 148
  NASA Langley Research Center
  Hampton, VA 23681–2199

NASA/TM–2016–218974

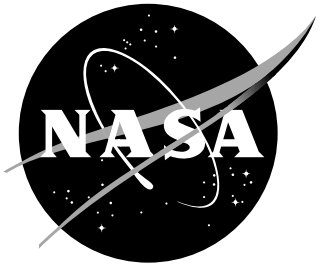

Compressive Testing of Stitched Frame and Stringer Alternate Configurations

Frank A. Leone, Jr.
NASA Langley Research Center, Hampton, VA

Dawn C. Jegley
NASA Langley Research Center, Hampton, VA

National Aeronautics and
Space Administration

Langley Research Center
Hampton, Virginia 23681-2199

April 2016

Acknowledgments

The authors would like to acknowledge the contributions of Ms. Teresa O'Neil for setting-up and performing the single-frame compression tests; Mr. George Cowley for setting-up and performing the single-stringer compression tests; and Dr. Nathaniel Gardner and Mr. Michael McNeill for setting-up and performing the optical measurements, and collecting and analyzing the data.

Abstract

A series of single-frame and single-stringer compression tests were conducted at NASA Langley Research Center on specimens harvested from a large panel built using the Pultruded Rod Stitched Efficient Unitized Structure (PRSEUS) concept. Different frame and stringer designs were used in fabrication of the PRSEUS panel. In this report, the details of the experimental testing of single-frame and single-stringer compression specimens are presented, as well as discussions on the performance of the various structural configurations included in the panel.

Contents

List of Figures

1 Introduction

As part of the NASA Environmentally Responsible Aviation (ERA) Project, researchers at NASA Langley Research Center (LaRC) and The Boeing Company (Boeing) worked together to develop technology to support lighter, more fuel-efficient commercial transport aircraft. A major milestone for the ERA Project was to design, build and test a 30-foot-long multi-bay box (MBB) test article that was representative of an 80%-scale center section of a hybrid wing body (HWB) vehicle. A sketch of the MBB with the forward upper and lower bulkhead panels removed is shown in figure 1. A detailed description of the steps in the multi-year process to develop this new lightweight composites concept is presented in reference 1.

The MBB test article contained 11 large, out-of-autoclave cured, carbon/epoxy panels built using the Pultruded Rod Stitched Efficient Unitized Structure (PRSEUS) concept [2]. PRSEUS is an enabling technology for HWB architectures, due to the ability of the concept to support a pressurized, non-circular fuselage efficiently for both cost and weight. The primary motivation for MBB development and testing was to demonstrate both the manufacturability for large-scale components and the performance and strength of the structure [3]. This new approach exploits the advantages of stitched composites by integrating the skin, frames, stringers, tear straps, and T-caps together into a single dry, self-supporting preform assembly. The integrated preform is then infused and co-cured in a single oven cure step using a vacuum-assisted resin transfer molding process with high-precision Invar outer mold line (OML) tooling. An exploded view of the intersection of a PRSEUS frame and stringer is shown in figure 2. Further details of the fabrication methodology for stitched composites are presented in reference 4.

The 11 stitched panels of the MBB test article were fabricated by Boeing at their facility in Huntington Beach, Calif., and subsequently assembled into the MBB at the Boeing C-17 final assembly facility in Long Beach, Calif. The MBB was tested in the Combined Loads Test System (COLTS) facility at LaRC in April through June 2015. The MBB was subjected to combinations of internal pressure loading and mechanical loading that were representative of the design limit loads and design ultimate loads of an HWB aircraft for various critical flight conditions. Testing of the MBB is documented in reference 5.

During fabrication of the panels for the MBB, ideas were developed about how to improve the design and further develop stitched structures for future applications. Therefore, an extra panel was fabricated to test some of these ideas. The primary motivation for fabricating this additional panel was to evaluate the structural performance of different configurations of the frames, stringers, and T-caps, as well as to develop the necessary fabrication processes and procedures for these new configurations.

This report focuses on a set of single-frame and single-stringer compression specimens that were harvested from the additional PRSEUS panel. This report presents details regarding the test specimens, the experimental procedure used to evaluate the specimens, and a discussion of the experimental results. Separate reports are available that focus on additional specimens harvested from the alternate center keel panel, including T-cap tension and bending specimens [6] and stringer rod push-out specimens [7].

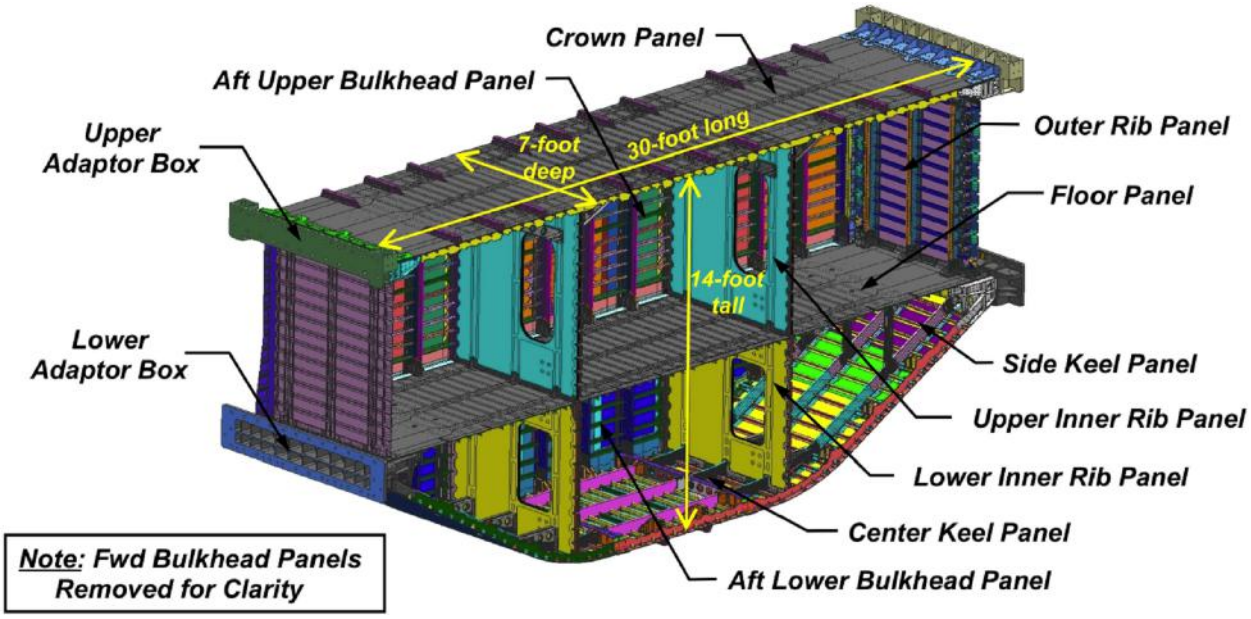

Figure 1: MBB test article components.

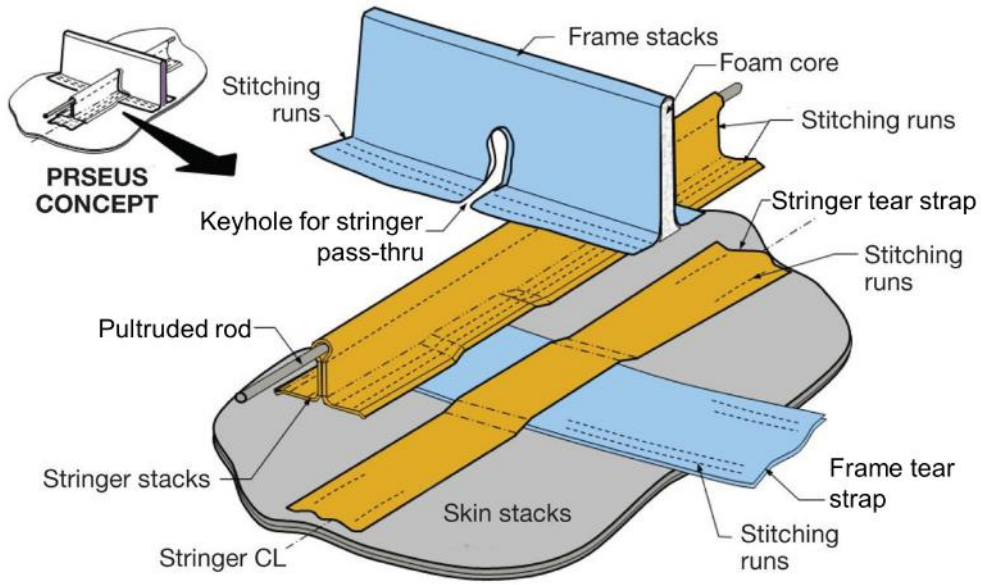

Figure 2: PRSEUS concept components.

2 Alternate Center Keel

A second center keel panel, based on the MBB center keel panel, was fabricated by Boeing and delivered to LaRC in February 2015. The inner mold line (IML) surface of this alternate MBB center keel panel is shown in figure 3. The panel measured 71.9-inches long and 75.4-inches wide. The panel was made from a combination of dry carbon warp-knit fabric, pultruded rods, foam core, and stitching threads.

The skin and most parts of the stiffeners were made from carbon fiber layers with a (44/44/12) fiber architecture, where the values are percentages of (0/±45/90) degree plies. This material grouping, known as Class 72, Type 1 pre-kitted stacks, was the same material used in the MBB [2]. Each of these stacks has a nominal cured thickness of 0.052 inches. Standard modulus Toho HTA40E13 carbon fibers were used in the Class 72 stacks. A second material grouping, known as Class 101, Type 3, was included in the alternate center keel panel. The Class 101 pre-kitted stacks have a stacking sequence of [+30/0/−30/0] and nominal cured thickness of 0.021 inch. IMS65 E23, Toho Tenax-E 24K intermediate modulus fibers were used in the Class 101 stacks. Multiple stacks of the warp-knit materials were used to build up the desired part stiffness, strength, and

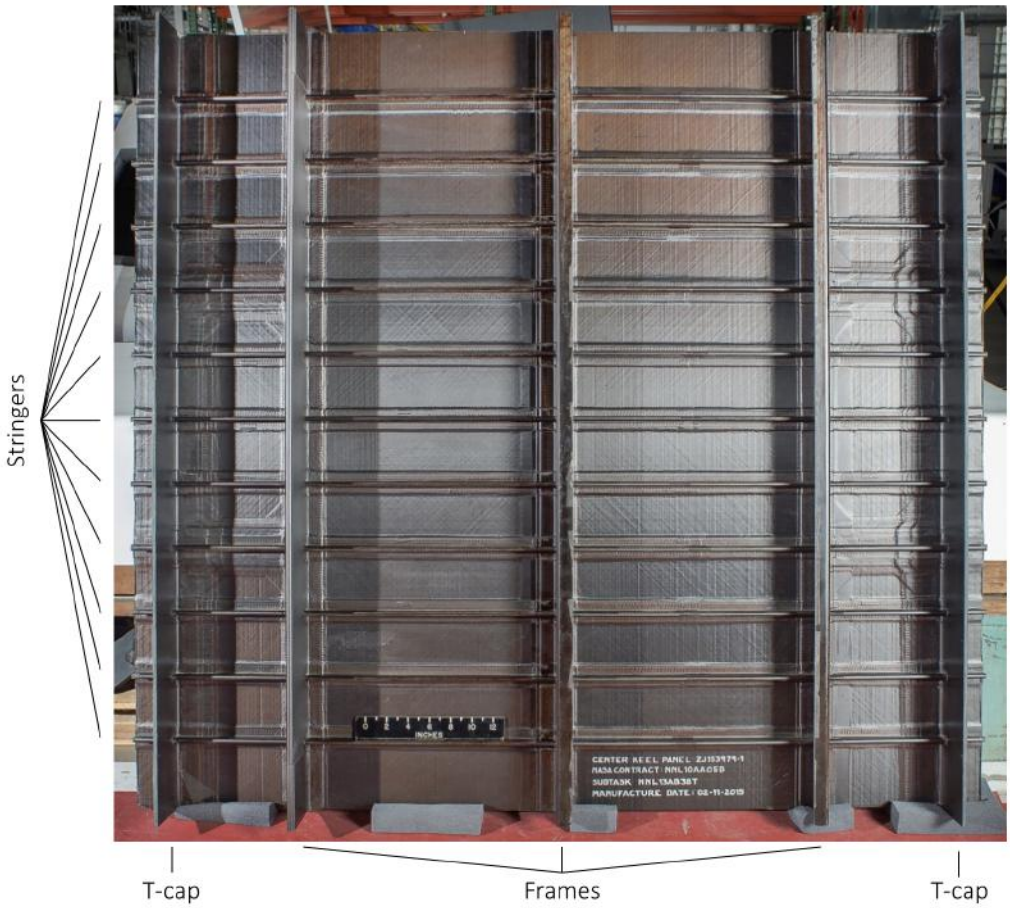

Figure 3: Photograph of the IML surface of the MBB alternate center keel panel, showing the stringers, frames, and T-caps.

configuration.

Through-the-thickness stitching was used to attach the stiffeners to the skin and, in selected locations, in the stiffener webs to form a dry, self-supporting preform. The preform was then infused with VRM-34 epoxy resin and cured in an oven. The panel contained three frames, 11 stringers, and two T-caps. Additional details regarding the design and fabrication of the alternate MBB center keel panel can be found in reference 8.

2.1 Frame and Stringer Configurations

Three frame configurations and five stringer configurations were included in the alternate center keel panel, as shown in figure 4. All three frames were composed of the Class 72, Type 1 pre-kitted stacks. The frame configurations evaluated in this study are:

- A foam-filled frame (labeled F1), identical to the MBB test article frames, which served as the baseline configuration. Two stacks of material were wrapped around a 0.5-inch thick Rohacell 110 WF foam core to form the F1 frame;
- A tapered-blade frame (labeled F2), with minimum gauge regions (i.e., one stack thickness) in the web and built-up regions around the keyhole at the frame/stringer intersections. Additional damage-arresting stitching was included in the frame web. This configuration was designed to be comparable to frames in conventional barrel fuselage; and
- A constant-thickness blade frame (labeled F3), with a uniform four-stack thickness, designed to be an alternative to the foam-filled frame for a HWB fuselage with damage-arresting stitching in the web.

Cross-sectional schematics of the three frame configurations are shown in figure 5. All of the frame and frame tear strap stacks were aligned in the 0° direction, with the 0° direction being aligned along the length of the frames. The F1 tear straps were 4.25-inches wide and the F2 and F3 tear straps were 3.75-inches wide. The skin of the alternate center keel panel was composed of a stack of Class 72 material with the same orientation as the frame and frame tear strap stacks. The F1 frames measured approximately 6.125 inches in height from the OML surface to the top of the frame. The F2 and F3 frames measured approximately 4.75 inches in height from the OML surface to the top of the frame. The top flange in the F2 and F3 solid frames measured 1.50-inches wide.

The weight per unit length for the F1, F2, and F3 frame configurations are 0.113 lb/in, 0.068 lb/in, and 0.092 lb/in, respectively. These values include the frame, the foam for the F1 configuration, and the frame tear strap, but not the skin. Because the cross-sectional areas of the frames are not constant along their lengths, these weights were calculated using the average cross-sectional area for one stringer-to-stringer volume (i.e., 6.0 inches in length).

A PRSEUS stringer consists of a tear-shaped, unidirectional, carbon rod contained within a carbon/epoxy overwrapping laminate. The overwrapping laminate also forms the web and bottom flange of the stringer. A schematic representation of a typical PRSEUS stringer cross-section which highlights each of these features is shown in figure 6. The five stringer configurations evaluated in this study varied in terms of stack material, stack orientation, and whether or not an adhesive layer was included between the rod and the overwrap. The five evaluated stringer configurations are:

- Class 72 overwrap (labeled S07, S10, S11);
- Class 72 overwrap with adhesive between the rod and overwrap (labeled S08, S09);
- Class 101 overwrap (labeled S01, S02, S05);
- Class 101 overwrap with adhesive between the rod and overwrap (labeled S03, S04); and
- Class 101 overwrap with a reversed stacking sequence (labeled S06).

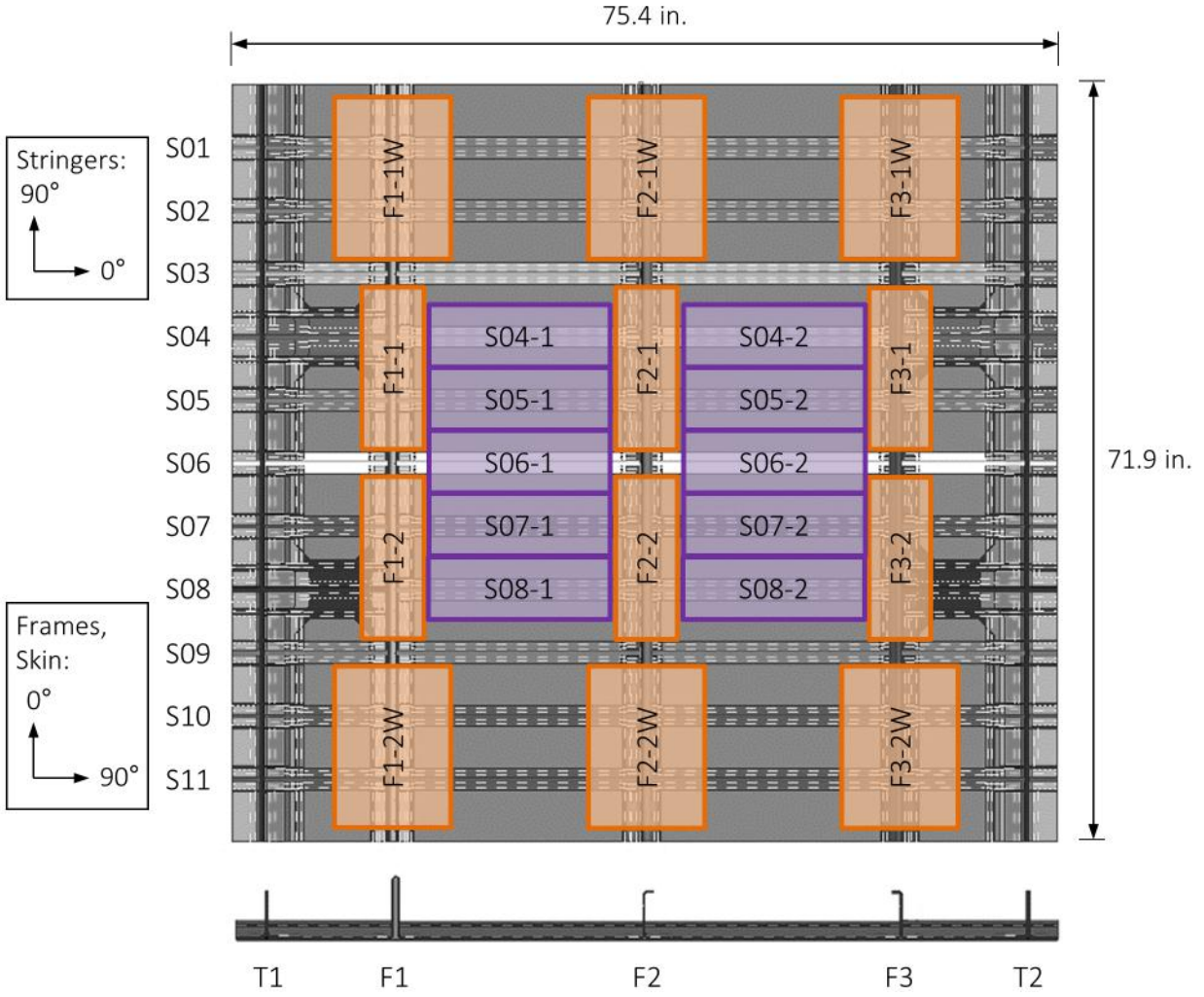

Figure 4: Single-frame compression and single-stringer compression specimen numbering and locations within the alternate center keel panel.

The default configuration of the Class 101 stacks (i.e., S04 and S05) had the outer 0° fibers placed inward toward the rod. The reversed stacking sequence (i.e., S06) had the +30° fibers placed inward toward the rod. The adhesive used between the rod and the overwrap in stringers S03, S04, S08, and S09 was Cytec FM300 adhesive. The layer of adhesive was 0.015-inch thick.

The Class 72 stringers had two stacks in the web and one stack in the overwrap. The Class 101 stringers had four stacks in the web and two stacks in the overwrap. All of the stringer and stringer tear strap stacks were aligned in the 0° direction, with the 0° direction being aligned with the length of the stringers. Consequently, the material stacks in the stringers and the skin were oriented 90° apart. The pultruded rods in the stringers were 0.375 inch in diameter, and composed of Grafil 34-700WD standard modulus carbon fibers and PUL6 epoxy resin, with a teardrop shape. Each stringer measured approximately 1.875 inches in height from the OML surface to the top of the stringer overwrap.

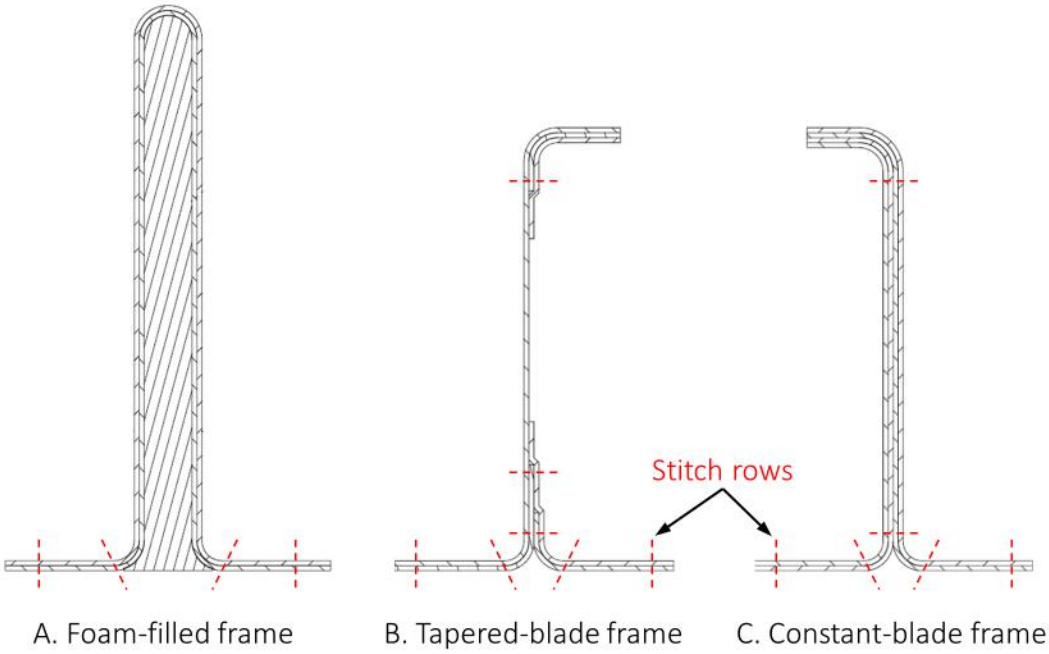

Figure 5: Cross-sectional views of the alternate keel panel frames. These cross-sections are representative of the frames between stringers. Additional doublers were used around the frame/stringer intersections in the tapered-blade frame.

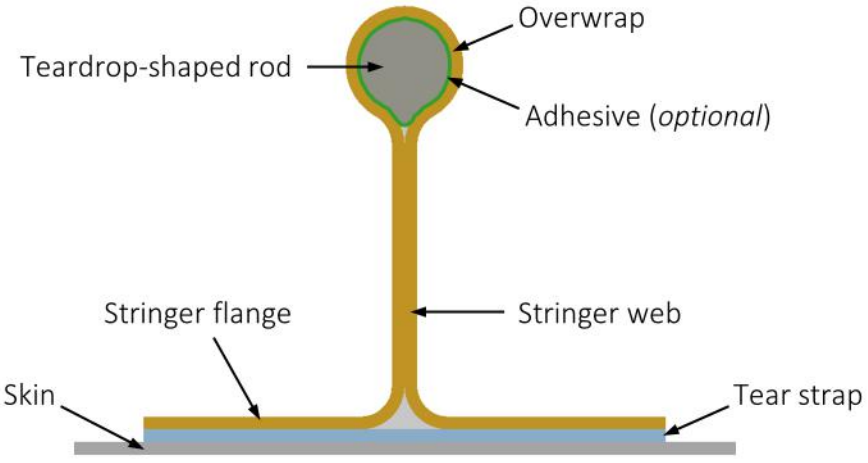

Figure 6: PRSEUS stringer cross-section.

2.2 Specimen Geometry

Twelve single-frame compression specimens were harvested from the alternate center keel panel. For each of the three frame configurations, two specimens were cut to a width of 5.7 inches and two specimens were cut to a width of 10.0 inches. The frame specimens are each 16.0 inches in length, and contain two stringers. Examples of the F1, F2, and F3 single-frame compression specimens are shown in figures 7, 8, and 9, respectively.

Ten single-stringer compression specimens were harvested from the alternate center keel panel. The stringer specimens are each 5.90 inches in width and 17.5 inches in length. An example of a single-stringer compression specimen is shown in figure 10. The numbering of the single-frame compression and single-stringer compression specimens and the locations from which they were taken in the alternate center keel panel are shown in figure 4.

One inch on each end of each compression specimen was potted in Hysol EA 9394 paste adhesive. The potted ends of the specimen are framed by a 1-by-7/8 inch welded steel angle, leaving 1/8 inch of unframed EA 9394 exposed on either end. The rectangular steel frames were sized so that at least 1 inch of potting material was between the specimen and the frame at all points.

Two pairs of back-to-back uniaxial strain gauges were installed on each specimen to check for proper specimen alignment during loading. All strain gauges were Micro-Measurements CEA-00-250UN-350 and had gauge factors of $2.065 \pm 0.5\%$. The gauges were aligned to measure strain in the loading direction. Each of the strain gauge pairs were installed 2.0 inches from the bottom of the specimens. The gauge pairs were installed symmetrically 1.5 inches from the centerline of the stringer for the stringer compression specimens, 1.0 inch from the centerline of the frame web for the 5.7-inch wide frame compression specimens, and 2.5 inches from the centerline of the frame web for the 10.0-inch wide frame compression specimens. The primary purpose of the installed strain gauges was to check for balanced load application during the tests.

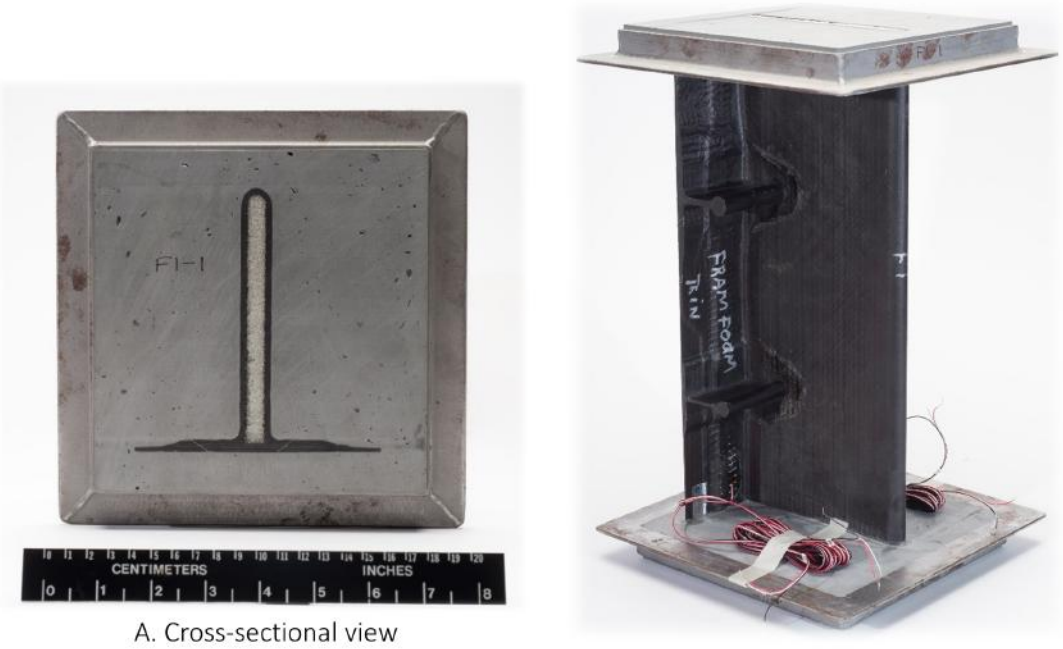

A. Cross-sectional view

B. Side view

Figure 7: Foam-filled frame specimen F1-1.

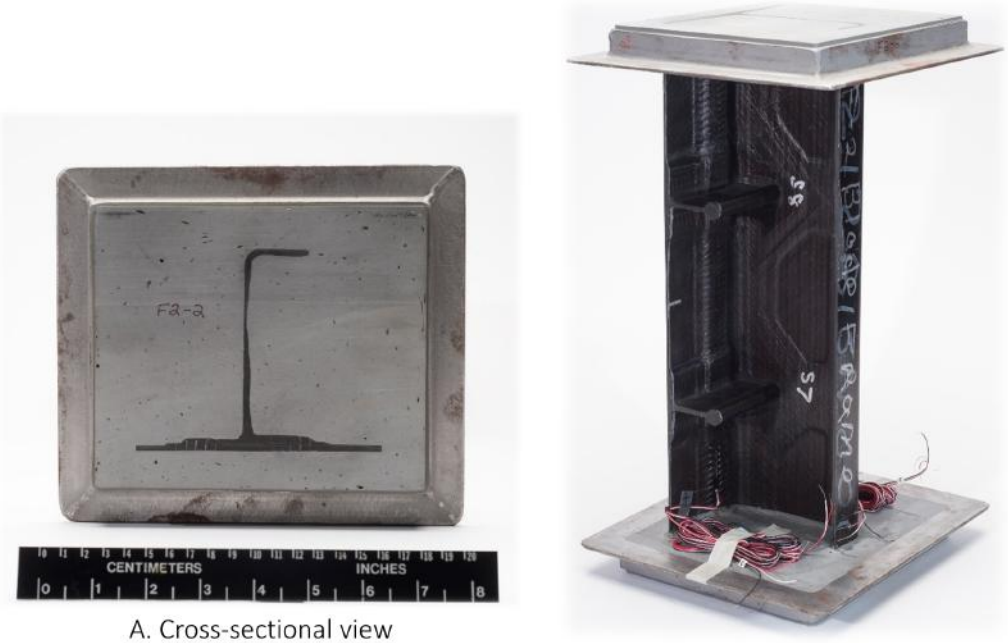

A. Cross-sectional view

B. Side view

Figure 8: Tapered-blade frame specimen F2-2.

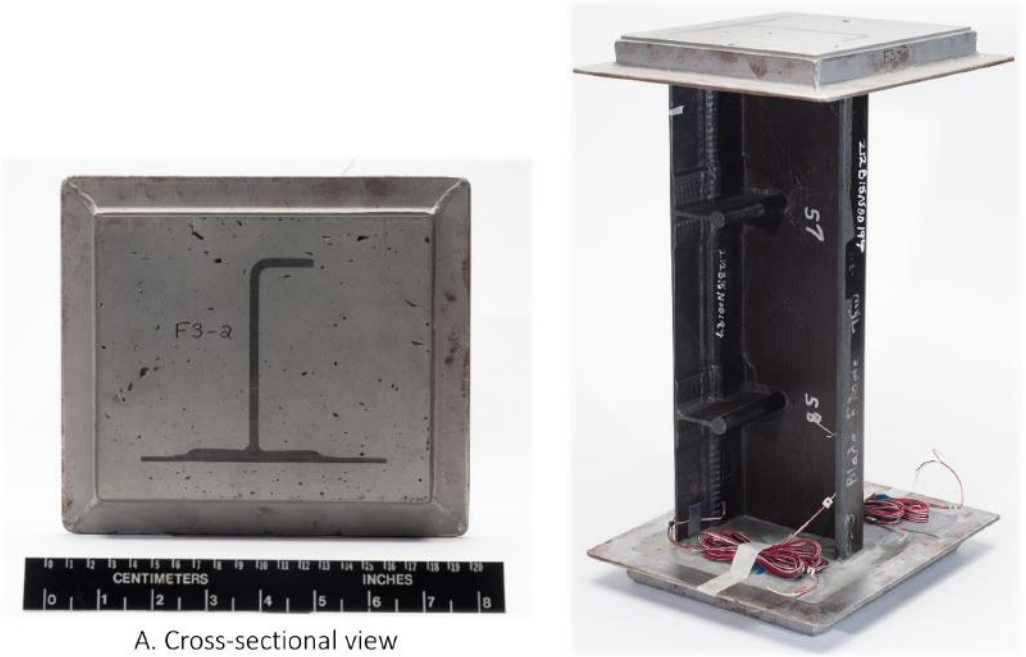

Figure 9: Constant-blade frame specimen F3-2.

Figure 10: Stringer specimen S08-1.

2.3 Experiment

The compression specimens were tested in a 120-kip load frame in the Structures and Materials Laboratory at NASA LaRC, shown in figure 11a. All tests were conducted at room temperature. The specimens were quasi-statically, monotonically loaded to failure under displacement control. A stroke rate of 0.008 inch/minute was used. The specimens were positioned so that the cross-section centroid of the stiffener/skin system was aligned with the center of the load platens and that the IML faced the wall behind the load frame.

In order to avoid premature buckling of the skin of the specimens in a global buckling mode, anti-buckling guides were used during the compression tests. Custom anti-buckling guides with gaps for the stringers were used for the single-frame compression tests. The anti-buckling guides were centered along the lengths of the specimens, leaving approximately equal gaps between the anti-buckling guides and the potting at each end.

The displacement and rotation of the top platen were monitored with three linear variable displacement transducers (LVDTs) during the tests, shown in figure 11b. The LVDTs used in the tests each had 0.25 inch of travel. The positions of the LVDTs on the top load platen, which were kept constant throughout the test campaign, are shown schematically in figure 12. The three vertical displacements measured by the LVDTs were used to define the applied displacement at the center of the specimen, rather than using the stroke output from the load frame.

The strain gauge, load cell, LVDT, and stroke data were recorded at a rate of 10 Hz during the tests. Strain gauge and load readings were zeroed before the top load platen was in contact with the specimens.

Two three-dimensional digital image correlation (DIC) systems were used to monitor the full-field deformation of the specimens during testing. The first DIC system (DIC 1 in figure 13) was equipped with Point Grey Grasshopper 5.0MP monochrome cameras, and was used to monitor the OML surface. Twenty-three-millimeter (mm) lenses were used during the frame compression tests and 17-mm lenses were used during the stringer compression tests. The second DIC system (DIC 2 in figure 13) was equipped with Point Grey Flea 2G 5.0MP monochrome cameras with 35-mm lenses, and was used to monitor one side of the stiffener. For the F2 and F3 single-frame compression specimens, the second DIC system monitored the flat side of the stiffener. During the tests, the out-of-plane displacement and loading direction strain were monitored to check for buckling and local material failure, respectively. Images were captured at a rate of one frame per two seconds. Prior to testing, the regions to be monitored by the DIC systems were spray painted with a flat, black-on-white speckle pattern, typical of DIC setups. The regions monitored by the two DIC systems were illuminated with white light-emitting diode (LED) lights during the tests.

A Vision Research Phantom v311 digital high-speed camera was used to monitor one side of the stiffener, positioned opposite the second DIC system. A 28-mm Schneider lens was used. Because the exact location of failure was a priori unknown, the full lengths of the frame and stringer specimens were monitored during loading. The image capture rates varied from 60,000 to 100,000 frames per second, depending on the field of view required for each specimen type. Prior to testing, the region to be monitored by the high-speed camera was spray painted with a flat white paint to allow for easier detection of surface cracks. The region monitored by the high-speed camera was illuminated with red LED lights. In order to avoid light leakage between the high-speed camera setup and the second DIC setup, a cardboard partition was placed between them and attached to the top of the stiffeners.

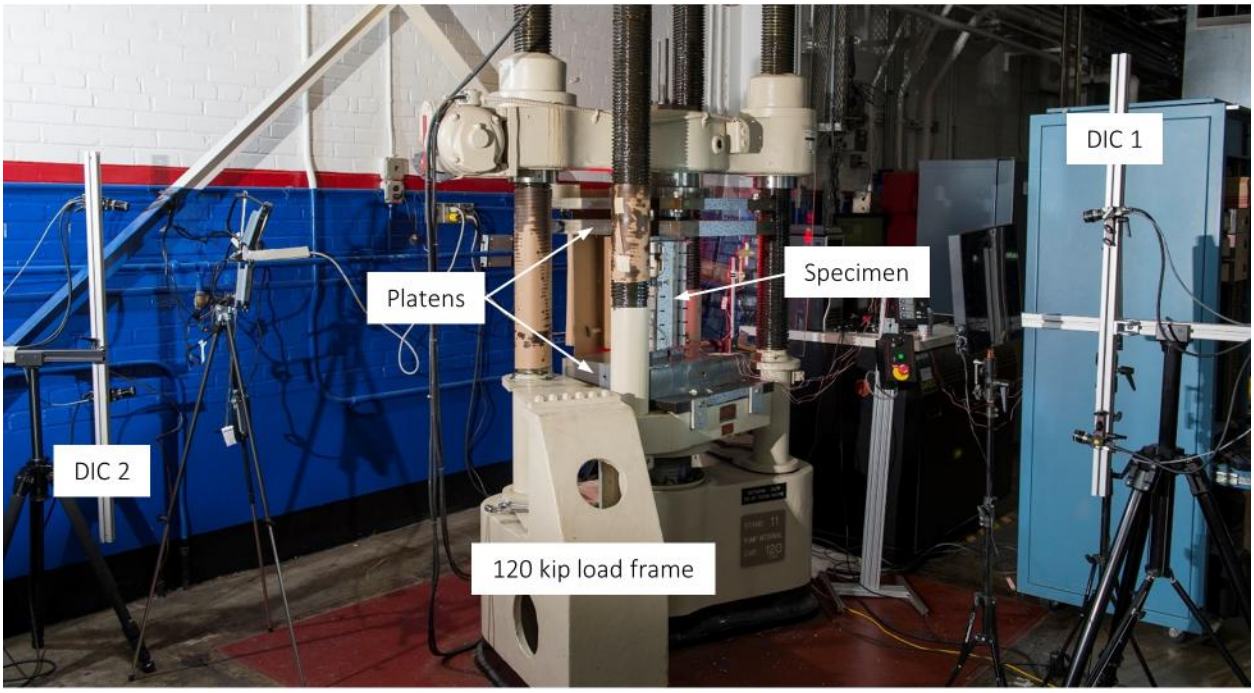

A. Load frame view

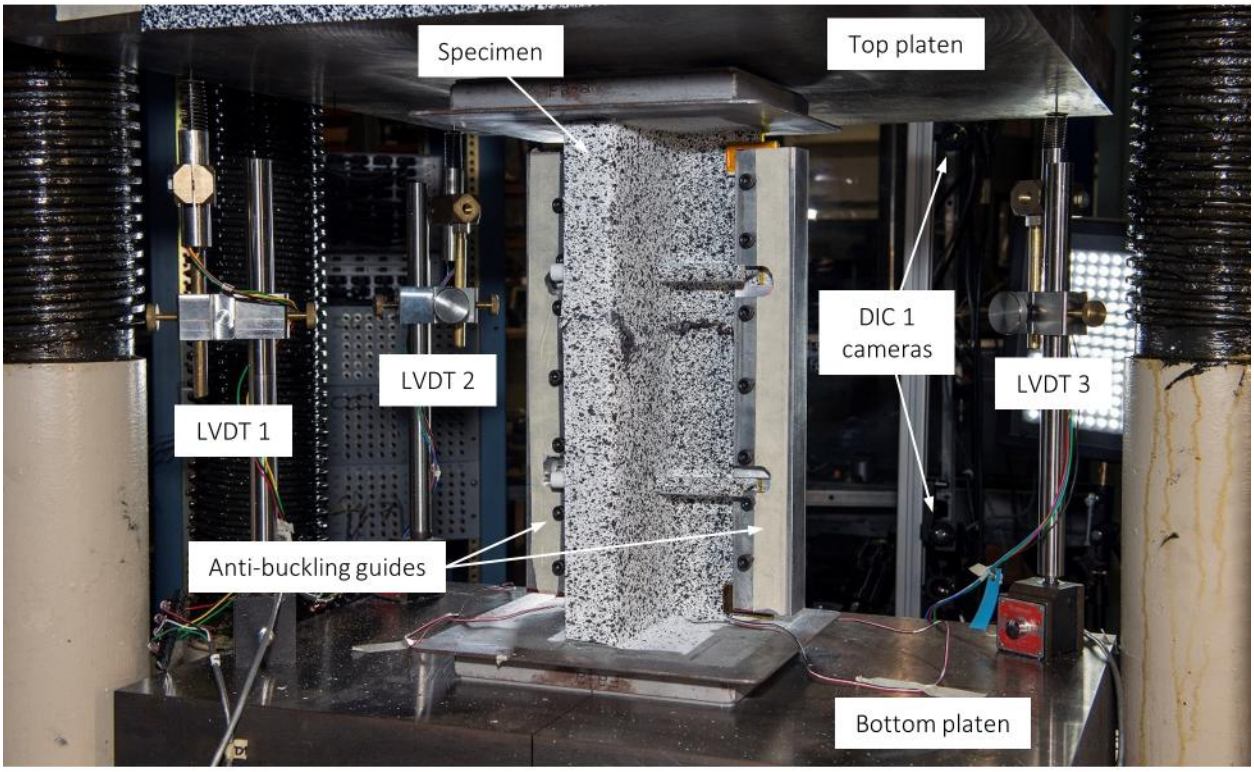

B. Specimen view

Figure 11: Experimental setup.

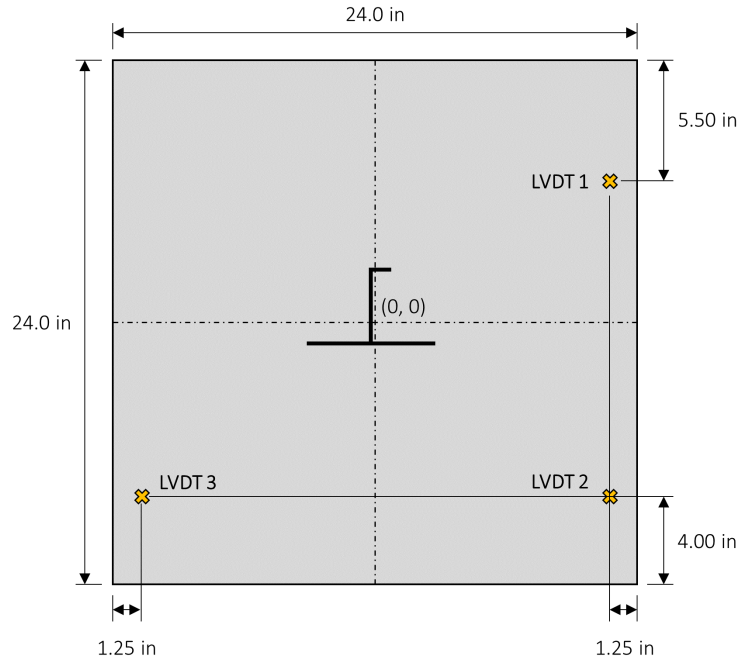

Figure 12: Positions of the three LVDTs on the top load platen.

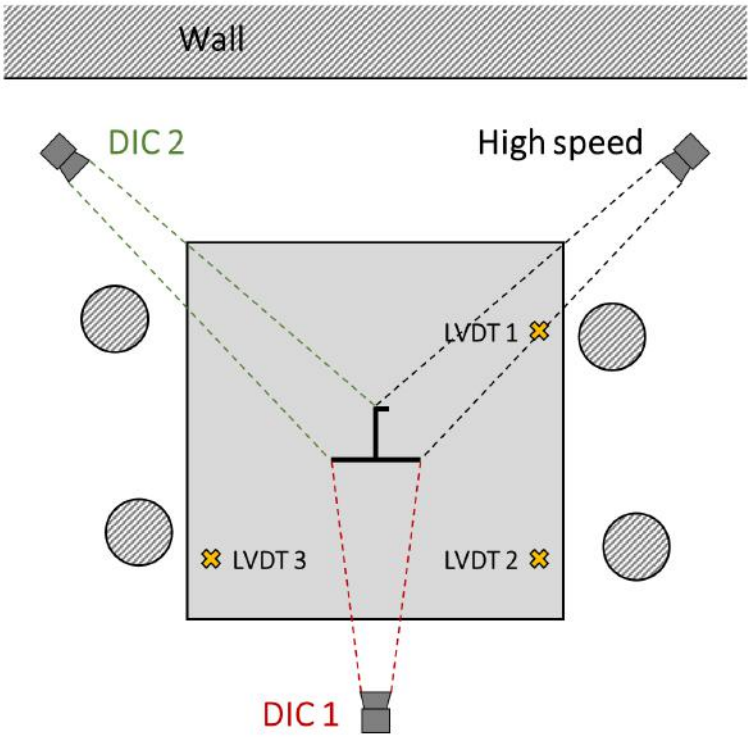

Figure 13: Measurement systems setup from the top-down view of the load frame.

3 Results and Discussion

3.1 Frame Specimens

Eleven out of 12 single-frame compression specimens were successfully loaded to failure. Specimen F3-2 was not able to be properly balanced in the load frame, and was, therefore, not tested. Despite having only two replicates per specimen configuration, the results were consistent for each specimen configuration in both stiffness and strength. In addition, the differences between replicates for a given configuration were generally smaller than the differences between specimen configurations.

A summary of the failure loads and stiffnesses of the single-frame compression specimens is presented in Table 1. The F1 specimens had the greatest strength and stiffness in both the narrow and wide configurations. The constant-thickness blade frame specimens (F3) had comparable stiffnesses to the F1 specimens, but the strengths of the F3 specimens were 16% lower in the narrow configuration and 14% lower in the wide configuration. As expected, the lighter F2 specimens yielded lower compression failure load, strength, and stiffness results than the heavier configurations. As mentioned, the F2 frame configuration was designed for a tube and wing configuration, not a HWB, and was not intended to carry compressive loads as high as the other two configurations.

Table 1: Single-frame compression results.

Specimen	Failure load [kip]	Strength* [ksi]	Stiffness [kip/in]
F1-1	−117.8	−58.3	1179
F1-2	−107.3	−53.0	1179
F1-1W	−92.0	−41.0	1235
F1-2W	−97.4	−43.4	1237
F2-1	−57.5	−39.5	847
F2-2	−49.7	−34.2	843
F2-1W	−61.2	−36.5	931
F2-2W	−59.5	−35.5	927
F3-1	−86.6	−46.8	1099
F3-1W	−70.1	−33.8	1182
F3-2W	−79.8	−38.5	1194

* Calculated using the specimen average cross sectional area, not including the foam in the F1 specimens.

The load-displacement histories for each of the tested single-frame compression specimens are shown in figure 14. The displacement in figure 14 is the displacement at the center of the top load platen, calculated using the positions and measured displacements of the three LVDTs. None of the specimens exhibited any major load drops prior to failing, with the exceptions of specimens F2-1 and F2-1W. All of the narrow frame specimens exhibited linear load-displacement behavior up to initial failure. Some load-displacement nonlinearity occurred in the wide F1 and F3 specimens beyond −60 kips, and beyond −30 kips in the wide F2 specimens.

Prior to failure, all of the frame specimens, narrow and wide, exhibited some degree of buckling within the minimum gauge skin sections along the edges of the specimens. The wide frame specimens developed clear half-waves located between the stringers, and between the stringers and the

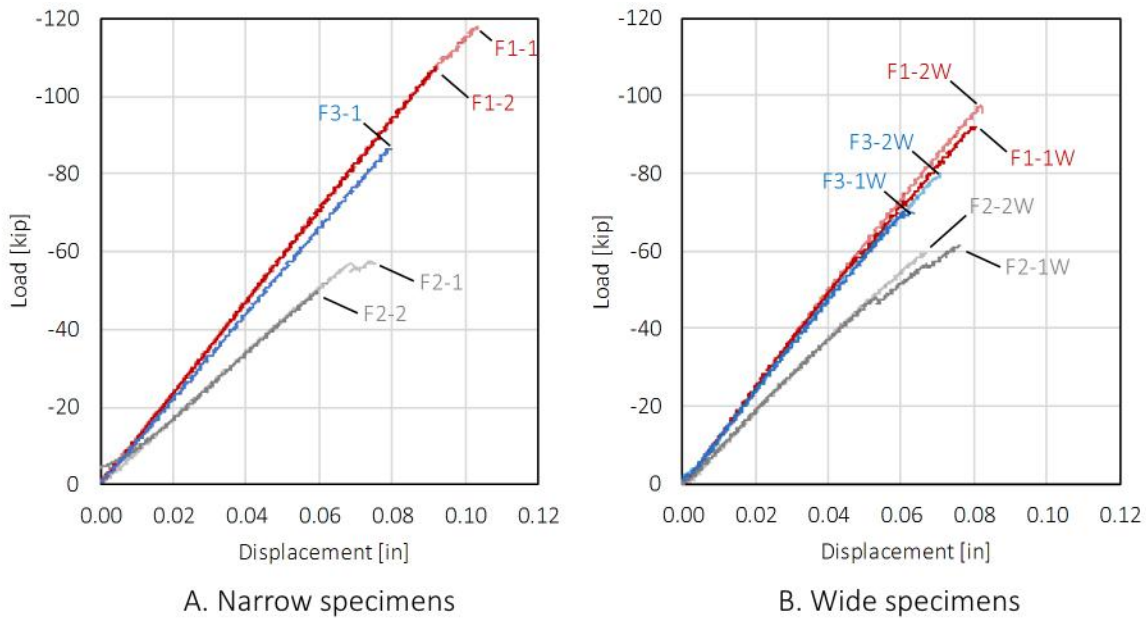

Figure 14: Frame compression specimen load-displacement responses.

potted ends of the specimens, as shown in figures 15a and 15b. The out-of-plane deformation of the narrow frame specimens was less consistent in terms of the number of half-waves and their locations along the specimen edges. Examples of the out-of-plane displacements of the narrow frame specimens are shown in figures 15c and 15d. The magnitudes of the out-of-plane displacements in the skin of the narrow specimens were consistently less than those of the corresponding wide frame specimens.

No buckling of the F1 or F3 specimen frame webs occurred during the tests. The F2 specimens, however, were prone to buckling in the frame webs due to their reduced thicknesses. Each of the four F2 frame specimens exhibited buckling within the frame webs in the forms of five half-waves along the specimen length. Specimen F2-1 exhibited one load drop at -56.6 kips applied load, which corresponded to the rapid change in the magnitudes and shape of the two half-waves closest to the top of the specimen, as shown in figure 16. Specimen F2-1W exhibited two small load drops. The second load drop occurred at -56.2 kips applied load, and corresponded to a similar change in the magnitudes of the three central half-waves, as shown in figure 17. The locations of ultimate failure for specimens F2-1 and F2-1W later corresponded to the locations of these buckling-mode shape changes.

The exact location and path of the final specimen failures varied across specimen configurations and across replicates. However, in all cases, the final damage state within the skin extended the full width of the specimen along either the edge of a stringer flange or beneath one-half of a stringer flange (e.g., figure 18); no dominant failures occurred in the skin between the stringers.

For the F1 and F3 specimens, the failure path in the stiffener tended either to be coplanar with the skin failure (e.g., figure 19a), or to pass through the stringer keyhole (e.g., figure 19b). For all of the F1 and F3 failures which were captured via the high-speed camera system, the failures originated at the root of the frame near the frame/stringer intersections, and propagated up the frame web. The failure process of specimen F3-2W is representative of the F1 and F3 specimens,

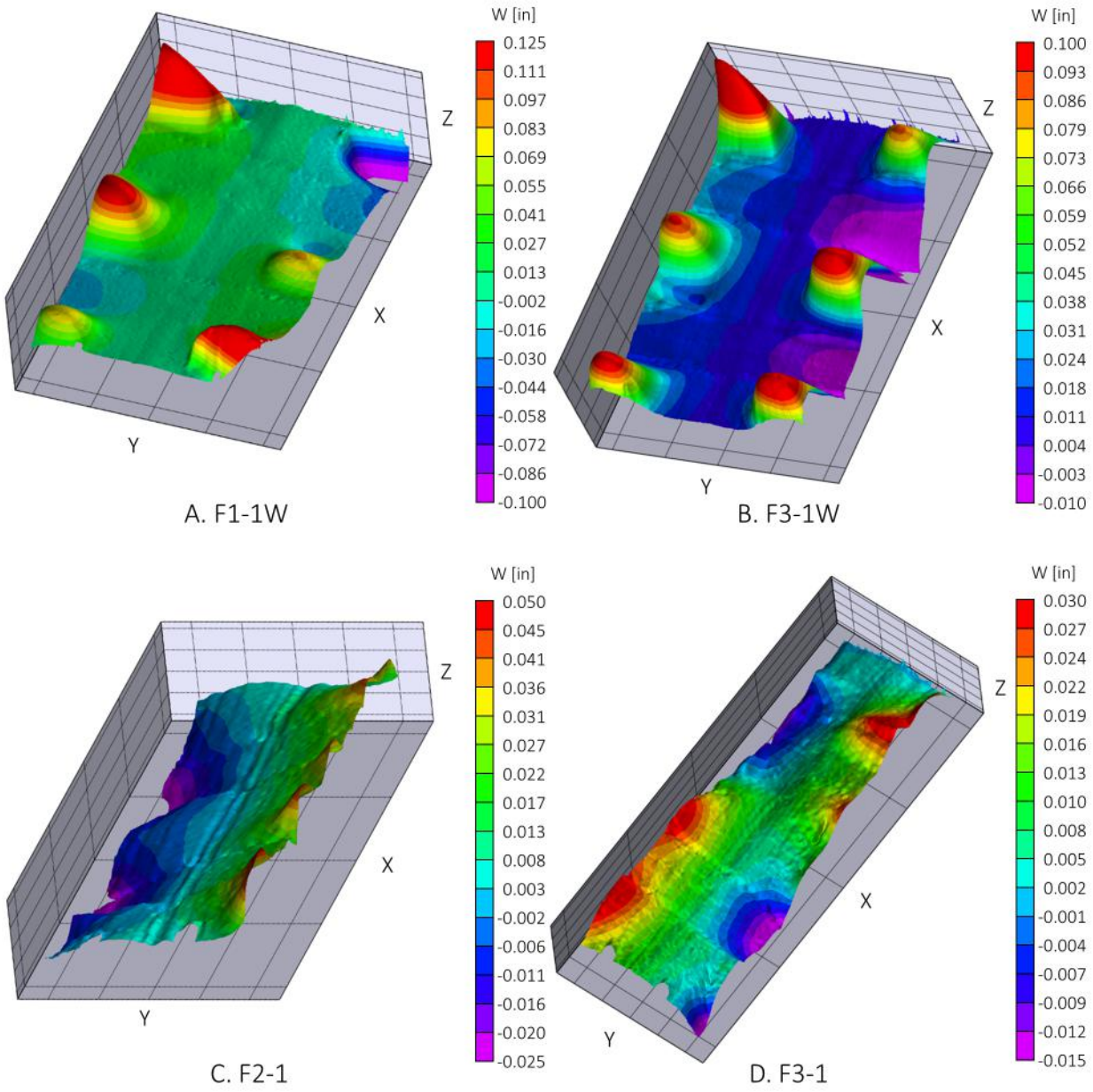

Figure 15: Out-of-plane skin deformation of selected frame specimens immediately before failure.

and is shown in figure 20. In the figure, select frames are shown in which significant changes in the damage state are visible. The time in microseconds (μs) between the first image and the subsequent images is shown in the subfigure captions.

For the F2 specimens, a combination of the built-up thickness around the stringer keyhole (visible in figure 8) and the through-the-thickness stitching prevented the failure path from passing through the keyhole. Instead, the observed failure paths connected the minimum gauge sections of the frame web and the stringer flange edges. The final F2 stiffener damage passed either between the two stringers (e.g., figure 19c) or between the potting and a stringer (e.g., figure 19d). The

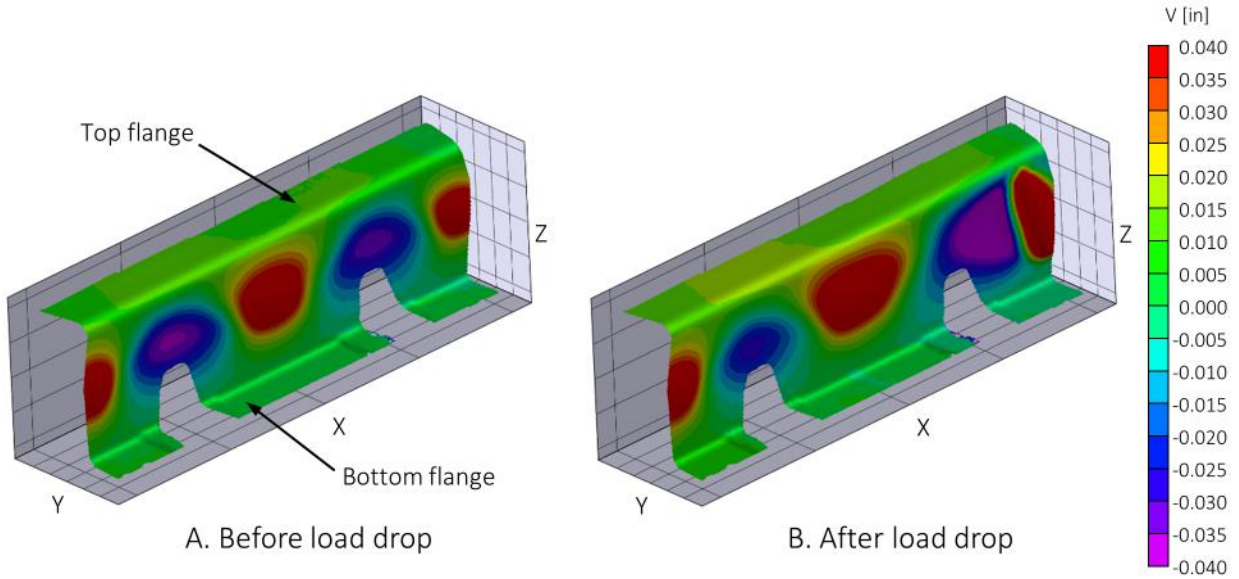

Figure 16: Out-of-plane deformation of the frame web in specimen F2-1.

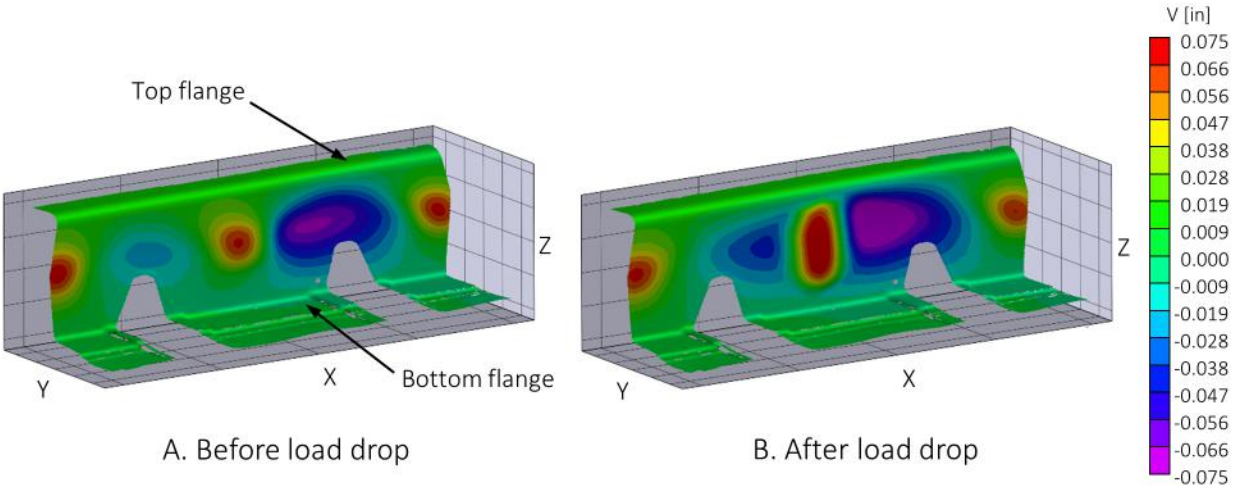

Figure 17: Out-of-plane deformation of the frame web in specimen F2-1W.

failure process of specimen F2-2W is representative of the F2 specimens, and is shown in figure 21. Damage was observed to initiate along the edge of the minimum-gauge region of the F2 frame web (figure 21b) and propagate along the stitch line along the stack termination in the frame web (figure 21c). The stitch line temporarily arrested the damage propagation (figure 21d) before ultimate failure (figure 21e).

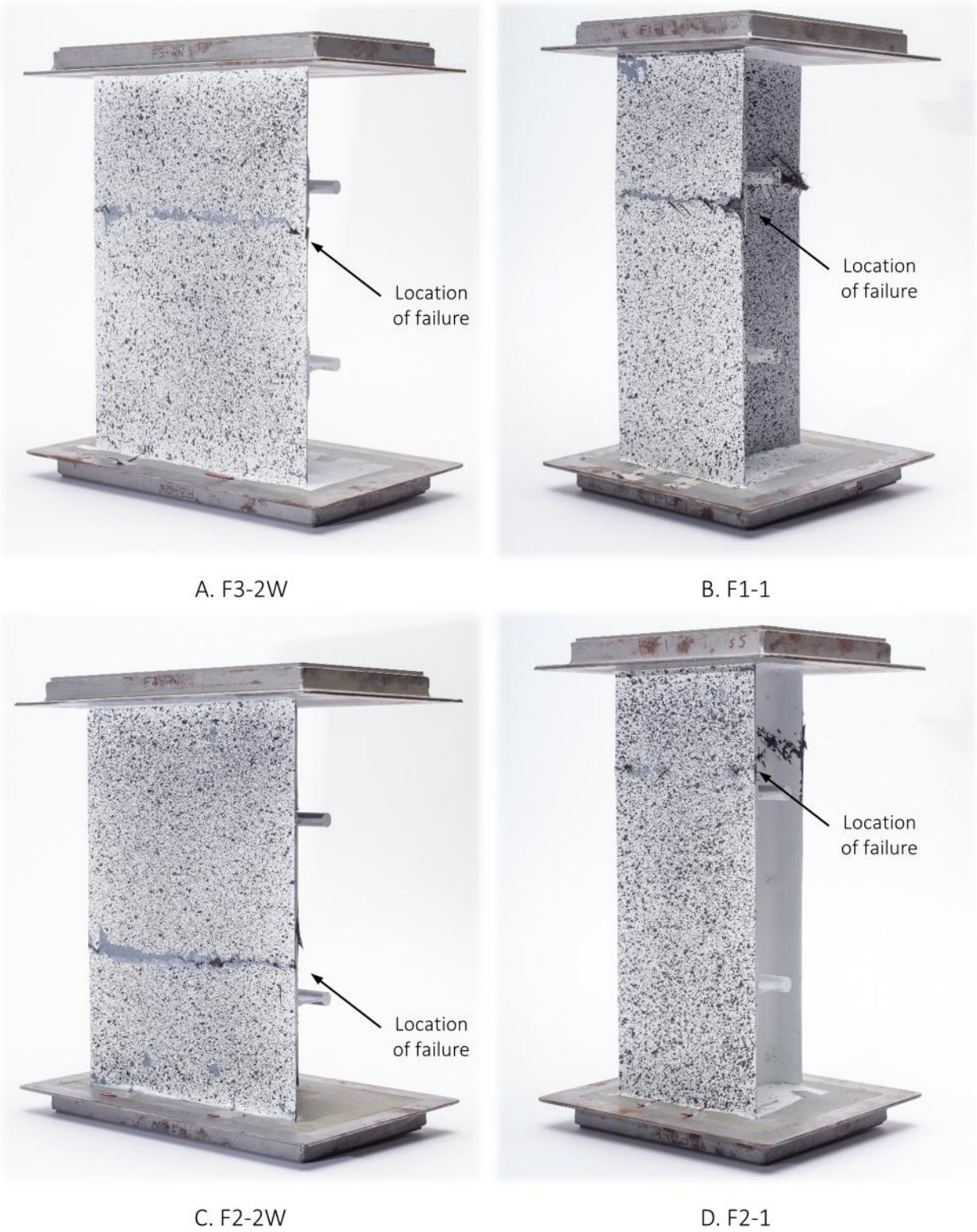

Figure 18: Locations of failure in the skins of a representative set of frame compression specimens, OML view.

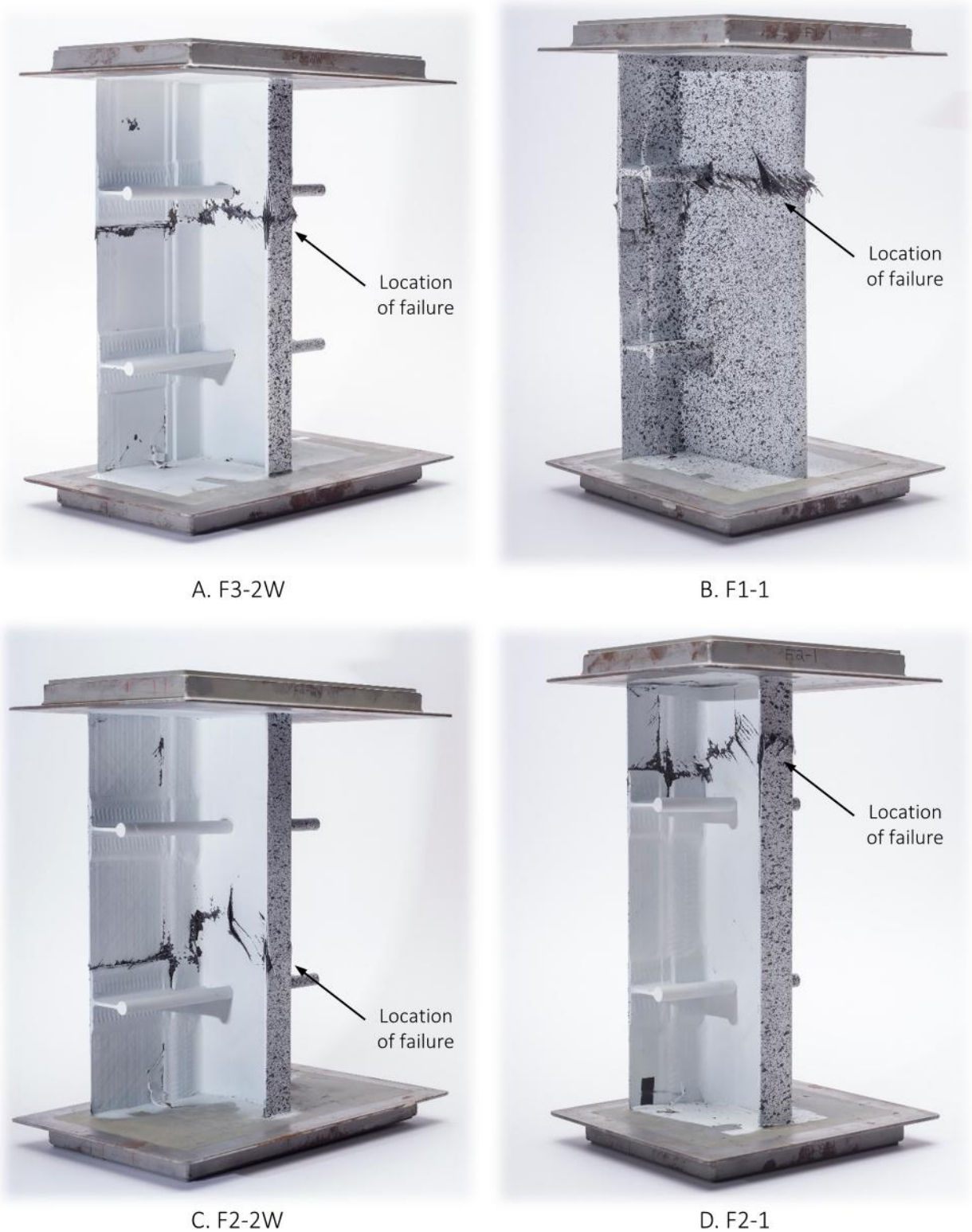

Figure 19: Locations of failure in the stiffeners of a representative set of frame compression specimens, IML view.

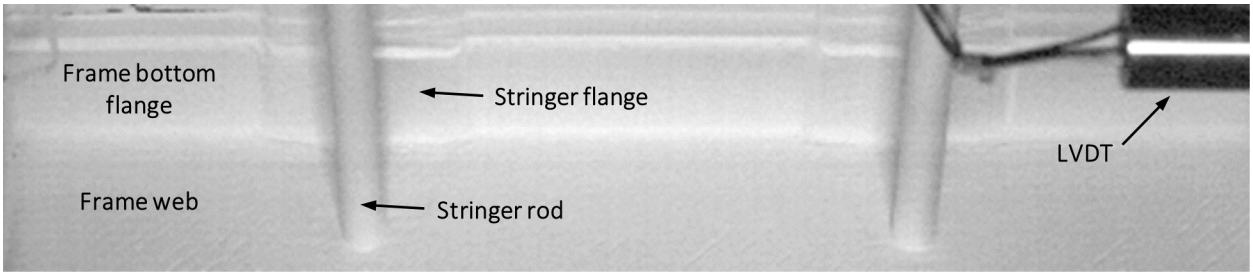

A. Δt = 0 μs

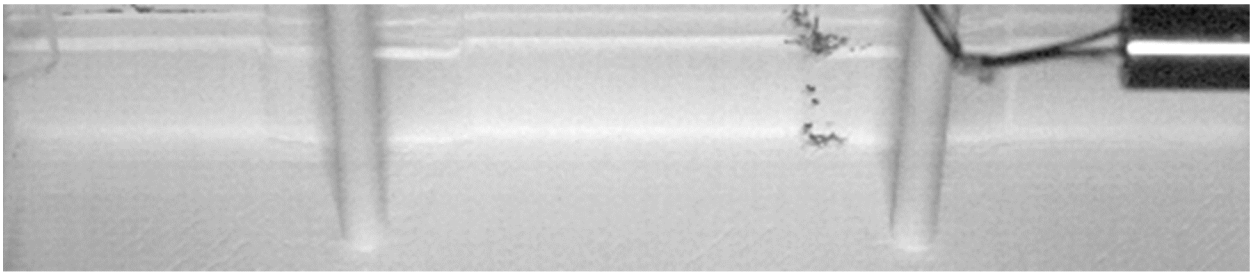

B. Δt = 166 μs

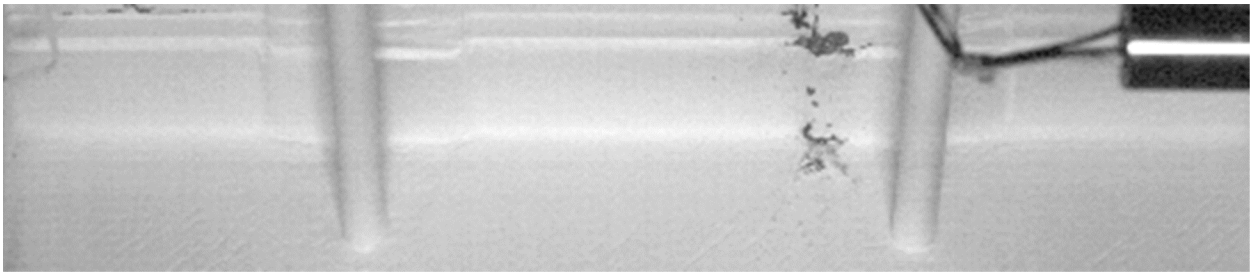

C. Δt = 1248 μs

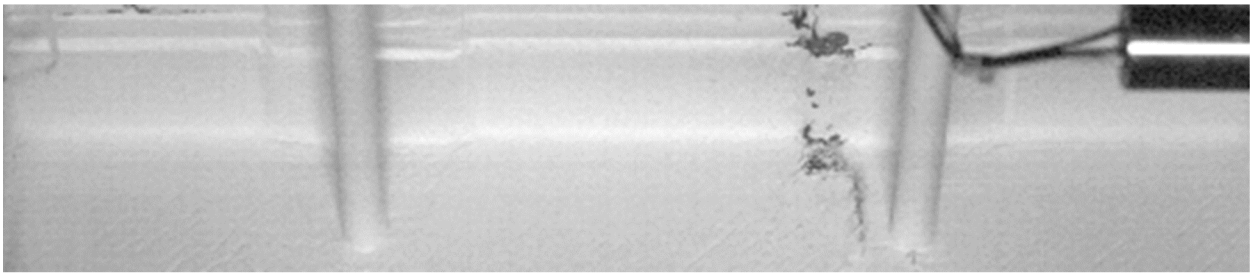

D. Δt = 1281 μs

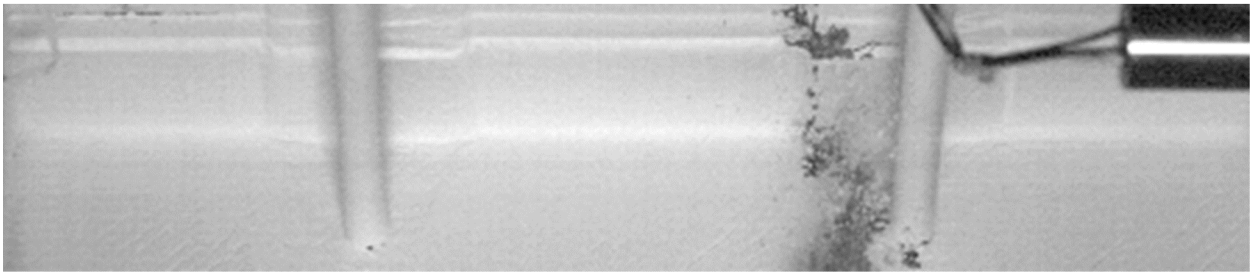

E. Δt = 1681 μs

Figure 20: High-speed photography images of the failure of specimen F3-2W.

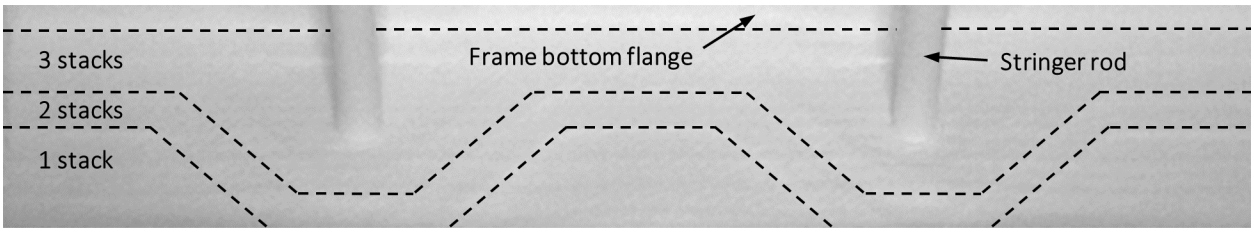

A. Δt = 0 μs

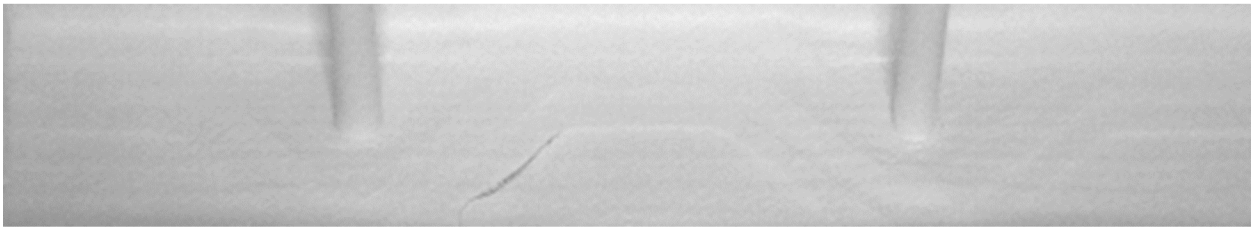

B. Δt = 100 μs

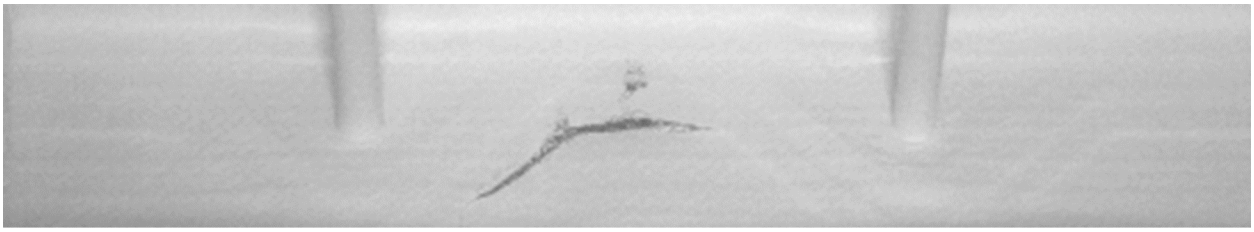

C. Δt = 329 μs

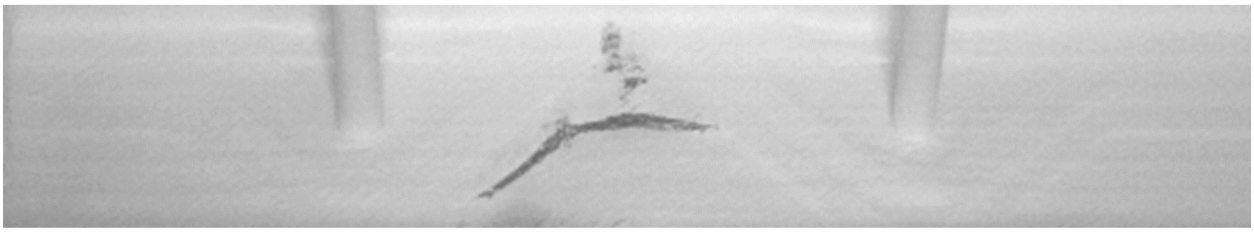

D. Δt = 629 μs

E. Δt = 3958 μs

Figure 21: High-speed photography images of the failure of specimen F2-2W. Stitch lines are located along the stack terminations in the web.

3.2 Stringer Specimens

All 10 single-stringer compression specimens were successfully loaded to failure. In all cases, prior to failure, the stringer exhibited global buckling. In nine out of 10 cases, the buckling load was the test peak load. A summary of the buckling loads, failure loads, and stiffnesses of the single stringer compression specimens is presented in Table 2.

Table 2: Single-stringer compression results.

Specimen	Buckling load [kip]	Failure load* [kip]	Stiffness [kip/in]
S04-1	−28.9	−28.4	466
S04-2	−32.1	−29.8	466
S05-1	−28.4	−29.6	471
S05-2	−28.0	−27.2	471
S06-1	−26.7	−25.8	469
S06-2	−28.2	−25.3	466
S07-1	−31.9	−29.4	414
S07-2	−32.0	−28.4	411
S08-1	−34.5	−29.3	412
S08-2	−35.2	−30.6	417

* The highest load reached after buckling.

The load-displacement responses for each single-stringer compression specimen are plotted in figure 22, separated by stringer configuration. While too few replicates were tested to make strong statements regarding the relative performance of the different stringer configurations, some trends are apparent from the experimental results.

In general, the Class 101 stringers were stiffer than the Class 72 stringers. In addition, the presence of adhesive between the rod and the stringer overwrap did not have any appreciable effect on the stringer stiffness for either material system, as expected. In terms of buckling load, the Class 72 stringers performed better than their Class 101 counterparts, with an average buckling load of −33.4 kips compared to −28.7 kips. The presence of the adhesive did not have an appreciable effect on the strength of the Class 101 specimens, but the Class 72 specimens with adhesive had buckling loads 9% higher than the Class 72 specimens without adhesive. The reversal of the stacking sequence of the Class 101 overwrap in stringer S06 did not significantly affect either the stiffness or buckling load of the specimens. However, the postbuckled failure loads of the S06 specimens were 11% lower than the other Class 101 specimens.

As mentioned, each of the single-stringer compression specimens buckled before ultimate failure. The buckling mode was the same for each specimen, with a single half wave along the length of the specimen, with the maximum deflection at the center. The pre- and post-buckled deformations of the stringer rod and web of stringer specimen S04-1 are shown in figures 23a and 23b, respectively. The stiffener buckling mode across the specimens varied only in terms of the right-or-left orientation of the central buckle. The stringer specimen skins did not buckle prior to the buckling of the stiffener. After the stiffener buckled, the skin on one side of the stiffeners was displaced toward the OML, while the skin on the opposite side was displaced toward the IML. The pre- and post-buckled deformations of the skin of stringer specimen S04-1 are shown in figures 23c and 23d, respectively.

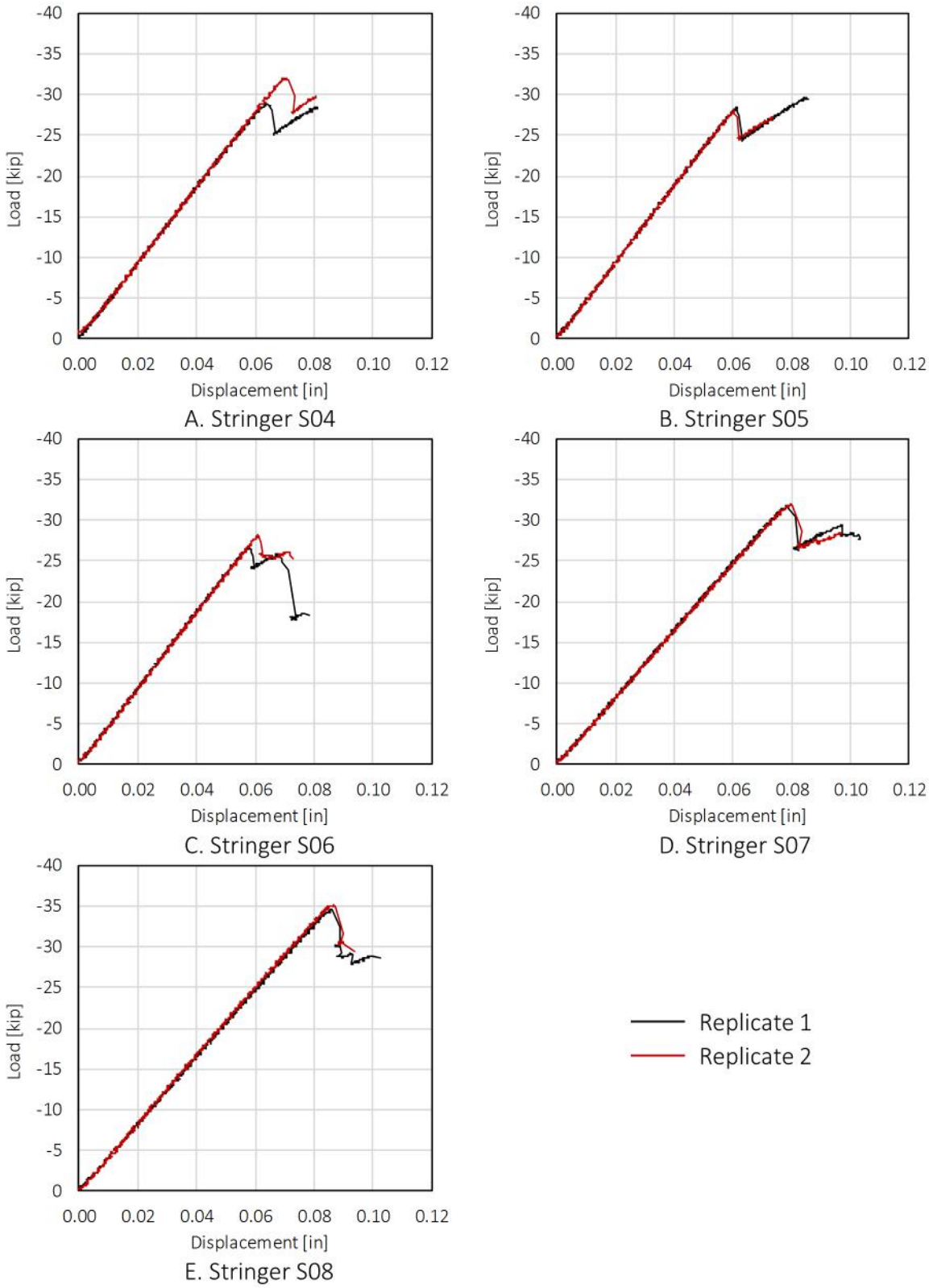

Figure 22: Stringer compression specimen load-displacement responses.

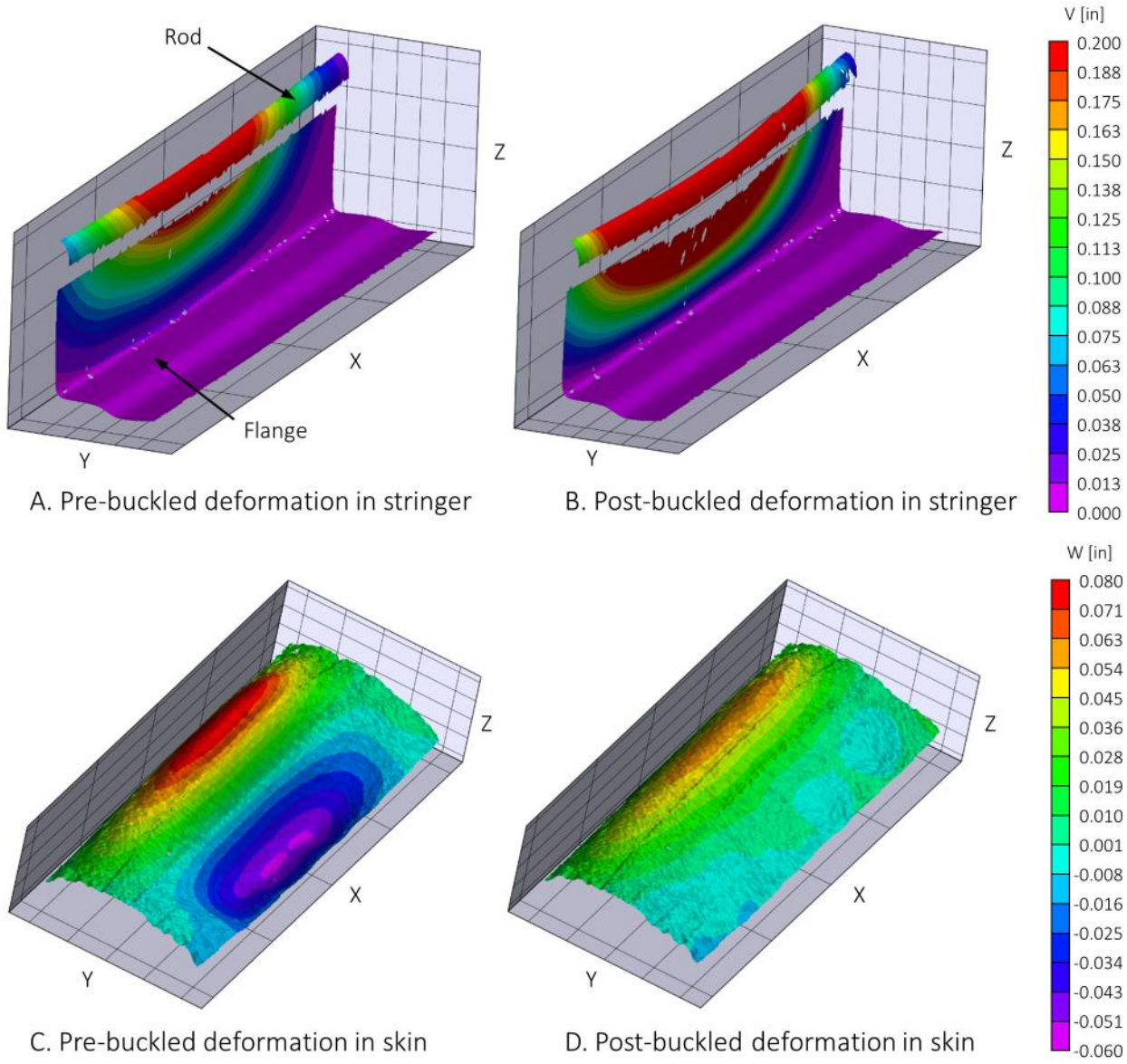

Figure 23: Pre- and post-buckled shapes of specimen S04-1.

A similar series of PRSEUS single-stringer compression tests are reported in reference 9. The stringers described in reference 9 contained the same rod and overwrap as stiffener S07 herein, but did not display buckling behavior, and their shortening behavior was linear to failure in the range of -40 kips to -45 kips applied load. However, in this previous work, the stringer height was only 1.5 inches, compared to the 1.875-inch tall stringers in the current study. In addition, in the previous work, the stacks in the skin had the same orientation as the stacks in the stringer, causing the previous specimens to be stiffer than those reported here. The difference in the stiffnesses of the skin and stringer herein likely contributed to the specimens buckling due to a greater portion of the overall load being carried by the stiffener.

Because the same general buckling behavior occurred for each stringer specimen, each of the

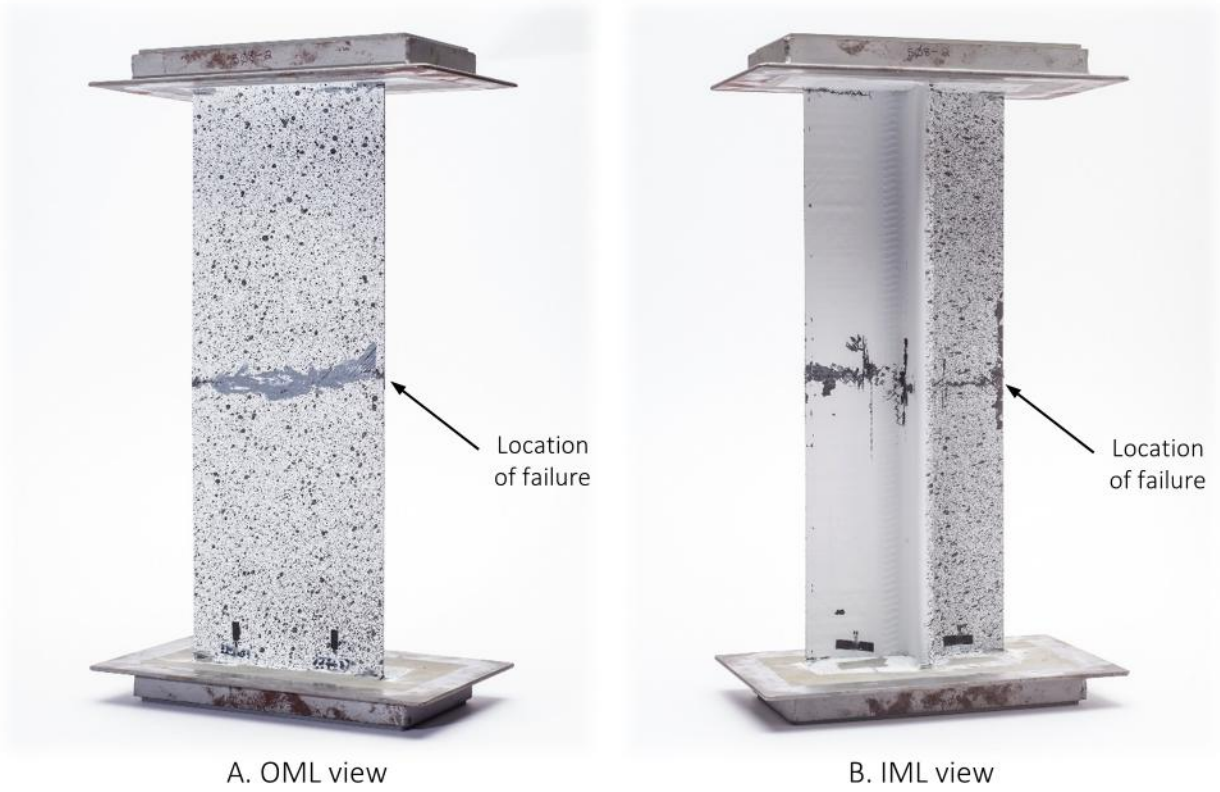

Figure 24: Post-test damage state for specimen S08-2.

stringer specimens failed at the same location: the center of the specimen length. The extent of post-test damage for specimen S08-2 is shown in figure 24. The visible post-test damage in the skin tended to be highly localized to a single plane normal to the loading direction. Typically, for co-cured or co-bonded skin and stringers, the entire length of the stringer delaminates/disbonds. [10] The stitching present in the tested specimens kept the failure zone localized.

The high-speed digital camera results revealed that the failures in the stringer specimens originated either at the fillets at the base of the stringer web or along the edges of the stringer flange. An example of failure propagation originating at the base of the stringer web is shown in figure 25 for specimen S04-1. The stiffener in specimen S04-1 buckled toward the second DIC system, causing the stringer rod to be out of frame at the bottom of the images in figure 25. Damage propagated from the base of the stringer web up toward the rod before also propagating through the skin. The damage in the stringer web propagated up and around the rod in most cases, though the rod itself was not observed to break.

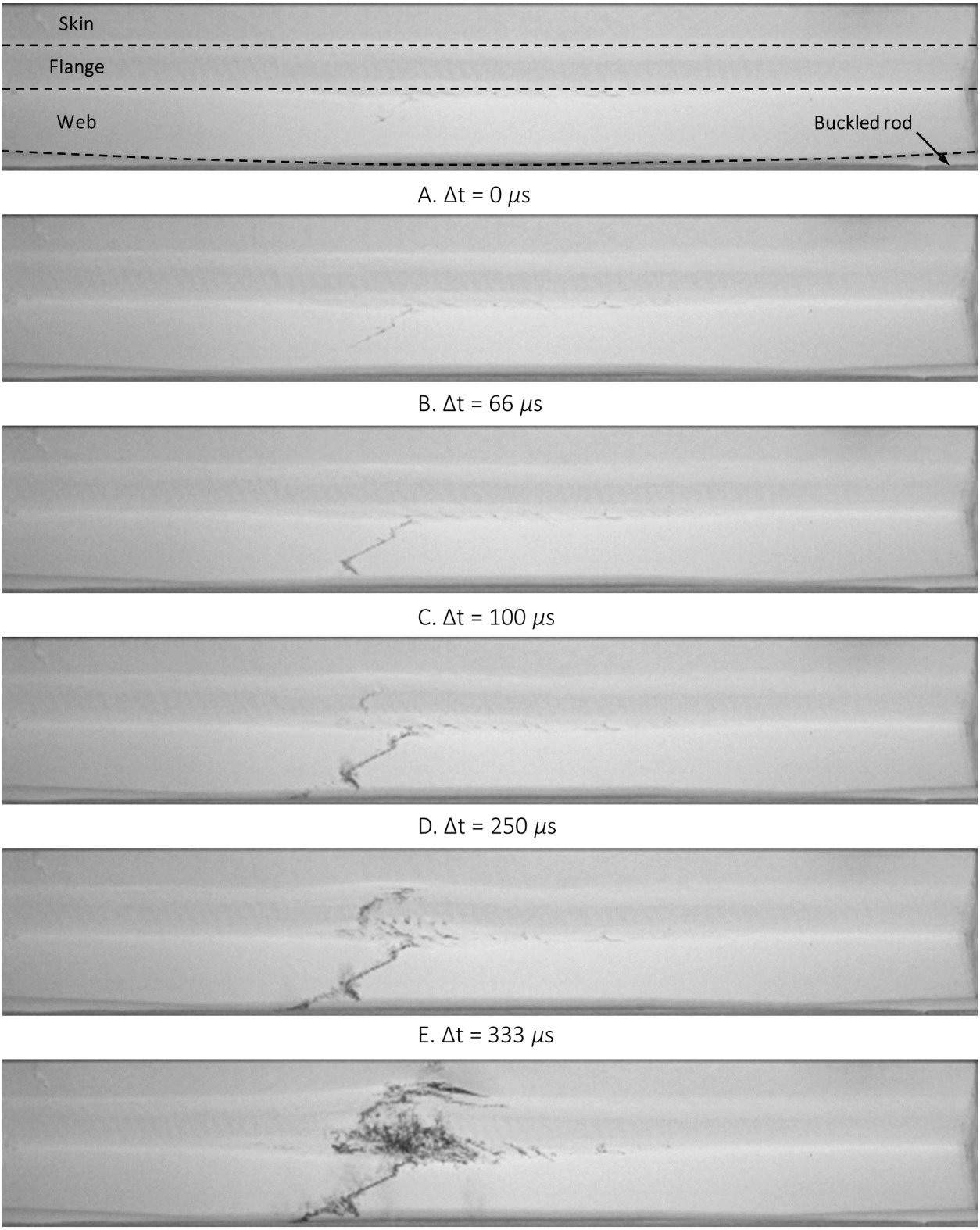

Figure 25: High-speed photography images of the failure of specimen S04-1.

4 Concluding Remarks

A series of tests were conducted on specimens harvested from a large stiffened panel containing a number of alternative design ideas for the application of the PRSEUS concept to frames, stringers, and T-caps. In this report, the details of a set of single-frame compression and single-stringer compression tests were presented. All of the tested specimens performed well within the behavior predicted from pre-test expectations and analyses, based on specimen weight (i.e., heavier frames failed at higher loads than lighter frames) and intended application (i.e., hybrid wing body versus conventional fuselage). None of the tested specimens exhibited any unforeseen failure processes.

Of the tested frame configurations, the constant-thickness blade frame performed comparably to the foam-filled frame configuration which was used in the MBB test article. This finding indicates that it may be possible to utilize the PRSEUS concept for HWB applications without involving foam in the frame. The thinner, lighter, tapered-blade frame post-buckled early in its load history, but continued to carry load without any load drops or severe nonlinearities until shortly before its ultimate failure.

The different stringer material configurations did not yield any significant differences in behavior. The tested specimens all exhibited buckling of the stringer to one side of the specimen, leading to failure at the center of the specimen at the point of maximum deflection. High-speed camera data revealed that the stringer failure process originated at the base of the stringer web.

References

1. Jegley, D.; and Velicki, A.: Status of Advanced Stitched Unitized Composite Aircraft Structure. *51st AIAA Aerospace Sciences Meeting including the New Horizons forum and Aerospace Exposition*, Grapevine, Tex., Jan. 2013.

2. Velicki, A.: Damage Arresting Composites for Shaped Vehicles, Phase I Final Report. NASA/CR-2009-215932, NASA Langley Research Center, Hampton, Va., Sept. 2009.

3. Velicki, A.; Yovanof, N.; Baraja, J.; Linton, K.; Li, V.; Hawley, A.; Thrash, P.; DeCoux, S.; and Pickell, R.: Damage Arresting Composites for Shaped Vehicles—Phase II Final Report. NASA/CR-2011-216880, NASA Langley Research Center, Hampton, Va., Jan. 2011.

4. Linton, K.; Velicki, A.; Hoffman, K.; Thrash, P.; Pickell, R.; and Turley, R.: PRSEUS Panel Fabrication Final Report. NASA/CR-2014-218149, NASA Langley Research Center, Hampton, Va., Jan. 2014.

5. Jegley, D.; Rouse, M.; Przekop, A.; and Lovejoy, A.: The Behavior of a Stitched Composite Large-Scale Multi-Bay Pressure Box. NASA/TM-2016-218972, NASA Langley Research Center, Hampton, Va., 2016.

6. Lovejoy, A.; and Leone, F.: T-cap Pull-off and Bending Behavior for Stitched Structure. NASA/TM-2016-218971, NASA Langley Research Center, Hampton, Va., 2016.

7. Leone, F.: Pultruded Rod/Overwrap Testing for Various PRSEUS Stringer Configurations. NASA/TM-2016-218975, NASA Langley Research Center, Hampton, Va., 2016.

8. Velicki, A.; Hoffman, K.; Linton, K.; Thrash, P.; Pickell, R.; and Turley, R.: Fabrication of Lower Section and Upper Forward Bulkhead Panels of the Multi-Bay Box and Panel Preparation. NASA/CR-2015-218981, NASA Langley Research Center, Hampton, Va., Nov. 2015.

9. Jegley, D.: Experimental Behavior of Fatigued Single Stiffener PRSEUS Specimens. NASA/TM-2009-215955, NASA Langley Research Center, Hampton, Va., Dec. 2009.

10. Jegley, D.; Velicki, A.; and Hansen, D.: Structural Efficiency of Stitched Rod-Stiffened Composite Panels With Stiffener Crippling. *49th AIAA/ASME/ASCE/AHS/ASC Structures, Structural Dynamics and Materials Conference*, Schaumburg, Ill., Apr. 2008.

REPORT DOCUMENTATION PAGE

Form Approved
OMB No. 0704-0188

1. REPORT DATE *(DD-MM-YYYY)*	2. REPORT TYPE	3. DATES COVERED *(From - To)*
01- 04 - 2016	Technical Memorandum	

4. TITLE AND SUBTITLE

Compressive Testing of Stitched Frame and Stringer Alternate Configurations

5a. CONTRACT NUMBER

5b. GRANT NUMBER

5c. PROGRAM ELEMENT NUMBER

6. AUTHOR(S)

Leone, Frank A.; Jegley, Dawn C.

5d. PROJECT NUMBER

5e. TASK NUMBER

5f. WORK UNIT NUMBER

338881.02.22.07.01.01

7. PERFORMING ORGANIZATION NAME(S) AND ADDRESS(ES)

NASA Langley Research Center
Hampton, VA 23681-2199

8. PERFORMING ORGANIZATION REPORT NUMBER

L-20631

9. SPONSORING/MONITORING AGENCY NAME(S) AND ADDRESS(ES)

National Aeronautics and Space Administration
Washington, DC 20546-0001

10. SPONSOR/MONITOR'S ACRONYM(S)

NASA

11. SPONSOR/MONITOR'S REPORT NUMBER(S)

NASA-TM-2016-218974

12. DISTRIBUTION/AVAILABILITY STATEMENT

Unclassified - Unlimited
Subject Category 39
Availability: NASA STI Program (757) 864-9658

13. SUPPLEMENTARY NOTES

14. ABSTRACT

A series of single-frame and single-stringer compression tests were conducted at NASA Langley Research Center on specimens harvested from a large panel built using the Pultruded Rod Stitched Efficient Unitized Structure (PRSEUS) concept. Different frame and stringer designs were used in fabrication of the large PRSEUS panel. In this report, the details of the experimental testing of single-frame and single-stringer compression specimens are presented, as well as discussions on the performance of the various structural configurations included in the panel.

15. SUBJECT TERMS

Compressive testing; Stiched; Stringer alternate

16. SECURITY CLASSIFICATION OF:			17. LIMITATION OF ABSTRACT	18. NUMBER OF PAGES	19a. NAME OF RESPONSIBLE PERSON
a. REPORT	b. ABSTRACT	c. THIS PAGE			STI Help Desk (email: help@sti.nasa.gov)
					19b. TELEPHONE NUMBER *(Include area code)*
U	U	U	UU	36	(757) 864-9658